American Mineralogist, Volume 69, pages 701–710, 1984

The heat capacities of osumilite from 298.15 to 1000 K, the thermodynamic properties of two natural chlorites to 500 K, and the thermodynamic properties of petalite to 1800 K

BRUCE S. HEMINGWAY, RICHARD A. ROBIE

U.S. Geological Survey, Reston, Virginia 22092

JAMES A. KITTRICK

Washington State University, Pullman, Washington 99164

EDWARD S. GREW

University of California, Los Angeles, California 90024

JOSEPH A. NELEN

Smithsonian Institution, Washington, D.C. 20560

AND DAVID LONDON[1]

Geophysical Laboratory, Carnegie Institution of Washington Washington, D.C. 20008

Abstract

We report results obtained with our recently automated low-temperature, adiabatic calorimeter. A brief description of the changes in the instrument are provided.

The heat capacities of natural osumilite ($K_{0.93}Na_{0.09}Ca_{0.02}Ba_{0.01}Mg_{1.88}Fe_{0.38}Ti_{0.01}Al_{4.62}Si_{10.12}O_{30}$) were measured from 340 to 1000 K by differential scanning calorimetry. The following polynomial fits the specific heat (J/g · K) of the natural sample with an average deviation of 0.5 percent between 298 and 1000 K.

$$C_P^\circ = 0.58332 + 1.2742 \times 10^{-3}T - 6.4871 \times 10^{-7}T^2 - 1.554T^{-0.5} - 3.961 \times 10^3T^{-2}$$

The heat capacities of two natural chlorites have been measured between 10 and 500 K. For the chlorite composition $(Si_{2.99}Al_{1.01})(Al_{1.39}Fe^{3+}_{0.21}\ Fe^{2+}_{0.57}\ Mg_{3.52})O_{10}(OH)_8$, the measured molar heat capacities, C_P°, between 200 and 500 K are consistent with the equation:

$$C_P^\circ = 1948.911 - 0.580880T + 2.0897 \times 10^{-4}T^2 - 2.298327 \times 10^4T^{-0.5} + 6.42272 \times 10^6\ T^{-2} \text{ (average deviation = 0.14\%).}$$

For the chlorite composition

$(Si_{2.47}Al_{1.53})(Al_{1.60}Fe^{2+}_{3.29}\ Mg_{1.05})O_{10}(OH)_8$ the polynomial

$$C_P^\circ = 3639.373 - 2.588354T + 1.26827 \times 10^{-3}T^2 - 4.564707 \times 10^4T^{-0.5} + 1.80322 \times 10^7T^{-2}$$

fits the measured molar heat capacities with an average deviation of ±0.36 percent. The heat-capacity values were not corrected for deviations from end member compositions. The entropy of the former phase is 431.7±5.0 J/(mol · K) and that of the latter is 495.7±10 J/(mol · K), both at 298.15 K. The reported entropy values do not contain a configurational entropy term and thus represent S_{298}–S_0.

[1] Present address: University of Oklahoma, Norman, Oklahoma 73019.

0003–004X/84/0708–0701$02.00

The entropy of petalite, $LiAlSi_4O_{10}$, is 233.2±0.6 J/(mol · K) at 298.15K. This result is in agreement with the value reported by Bennington et al. (1980, U.S. Bur. Mines Rept. Inv. 8451) of 232.2±2.0J/(mol · K).

The molar heat capacities of petalite between 200 and 1800 K are given by the polynomial

$$C_P^\circ = 876.26 - 0.20793T + 5.3009 \times 10^{-5}T^2 - 1.0691 \times 10^4 T^{-0.5} + 4.033 \times 10^6 T^{-2}$$

The average deviation of the fit is 0.17 percent. The results reported here were combined with the drop calorimetry data for petalite reported by Bennington et al. (1980) and with estimated values for temperatures greater than 1200 K.

Introduction

Thermodynamic data are particularly sparse for minerals that occur primarily in metamorphic terrains. Partly to ameliorate the situation, we measured the heat capacities of two natural chlorite samples and a natural osumilite sample. The data represent preliminary results in a continuing study of the thermodynamic properties of chlorites and osumilite.

We also report measurements of the heat capacities of petalite from 5 to 500 K and provide tables of the thermodynamic properties of petalite to 1800 K. Bennington et al. (1980) have determined the enthalpy of formation at 298.15 K, the heat content from 402 to 1194 K, and the heat capacity from 10 to 302 K for a natural petalite sample. Our measurements were undertaken prior to the publication of the results of Bennington et al. and in support of research arising from the dissertation studies of David London (1981).

Materials

The osumilite was separated from a granulite collected at Gage Ridge, Enderby Land, Antarctica (sample 2045C). A chemical analysis (the average of 10 microprobe analyses) is provided in Table 1 (details given in Grew, 1982). The sample was a 35.621 mg split that had been hand picked and washed in warm dilute HCl. Grew (1982) discussed in detail the petrology of Enderby Land including sample 2045C.

Kittrick (1982) obtained in excess of 100 g samples of two natural chlorites from Wards Natural Science Est.[2] and determined the polytype of each to be IIb (e.g., Bailey, 1975, p. 242). Chemical analyses for Si, Al, Ti, Fe, Mn, Ca, Mg, K, Na and P were made with an X-ray spectrograph by Dr. Peter Hooper (Washington State Univ.). Fe^{2+} and Fe^{3+} were determined by Kittrick with orthophenanthroline after HF decomposition (e.g., Roth et al., 1968). The results of these analyses (normalized and excluding volatiles) are given in Table 1. Each sample was subjected to combinations of Mg and K saturation, heating, and glycerol solvation and was followed by X-ray diffraction analysis of oriented samples allowing Kittrick (1982) to determine that no other detectable phase was present in the samples.

The unit-cell formulas were calculated according to an 18 oxygen unit cell (e.g., Jackson, 1969) by Kittrick (1982). The resulting chlorite compositions are $(Si_{2.99}Al_{1.01})(Al_{1.39}Fe^{3+}_{0.21}Fe^{2+}_{0.27}Mg_{3.52})O_{10}(OH)_8$ for the high-Mg chlorite from Quebec labeled 21-C and $(Si_{2.47}Al_{1.53})(Al_{1.60}Fe^{2+}_{3.29}Mg_{1.05})O_{10}(OH)_8$ for the high-Fe chlorite from Ishpeming, Michigan labeled 21-D. For convenience, the samples will be referenced throughout this paper by these labels.

The natural petalite sample (USNM 149544) was supplied by David London who obtained the sample from a mineral dealer.

Table 1. Chemical analyses for osumilite, two natural chlorites (normalized results) and petalite. (n.a., not analyzed)

	Osumilite* Gage Ridge, Antartica 2045C	Chlorite** Quebec 21-C	Chlorite** Ishpeming, Michigan 21-D	Petalite*** Minas Gerais, Brazil USNM 149544
SiO_2	61.50	35.53	21.88	78.37
Al_2O_3	23.84	24.36	23.64	17.06
TiO_2	0.10	0.10	2.42	0.02
Fe_2O_3	0.15	5.41	17.12	[<0.01
FeO	2.62	6.20	19.60	[
MnO	0.02	0.08	0.13	<0.01
CaO	0.10	0.00	4.43	<0.02
MgO	7.67	28.32	6.52	<0.01
K_2O	4.41	0.00	0.26	<0.01
Na_2O	0.28	0.00	1.00	<0.01
Li_2O	*	n.a.	n.a.	4.35
P_2O_5	n.a.	0.01	3.01	<0.01
BaO	0.15	n.a.	n.a.	n.a.
H_2O^-	n.a.	n.a.	n.a.	0.04
H_2O^+	n.a.	n.a.	n.a.	0.09
Total	100.84	100.01	100.01	99.93

* The average of 10 microprobe analyses. Fe^{2+} and Fe^{3+} determined by Mossbauer data. Semi-quantitive emission spectrographic analysis indicated that the amounts of Ba, B, Ca, Co, Cu, Ga, Pb, Ni, Ta, Sn, V, Zn, Mn, and Li do not exceed 0.05 weight percent. Details are given in Grew (1982).

** X-ray spectrographic analysis where iron is arbitrarily recorded as 44% Fe_2O_3 and 56% FeO. By wet chemical procedures: for sample 21-C, of the 8.63 percent iron, 6.31% is Fe^{2+} and 2.32 percent is Fe^{3+}; for sample 21-D, all iron was found to be Fe^{2+}.

*** Spectrographic analysis with H_2O by ignition loss.

[2] The use of trade names is for descriptive purposes only and does not imply endorsement by the U.S. Geological Survey, Washington State University, The University of California, The Smithsonian Institution, or the Carnegie Institution of Washington.

The general source of the material was a pegmatite in the state of Minas Gerais, Brazil. The petalite is water-clear and colorless, free of inclusions, and reportedly is derived from a single giant crystal that occurred in a pegmatitic pocket. The sample was a portion of the material used by London and Burt (1982) and London (1981). The sample used for the heat-capacity measurements was lightly crushed. Material less than 100 mesh was removed by dry seiving. A chemical analysis of the sample is given in Table 1.

Apparatus

The hardware in the low-temperature adiabatic calorimeter and the differential scanning calorimeter have been described elsewhere (Robie and Hemingway, 1972; Robie et al., 1976; and Krupka et al., 1979). The provisional temperature scale used in the laboratory was discussed by Robie et al. (1978). These components of the calorimetric systems remain unchanged.

The electrical measurement circuit of the low-temperature calorimeter has been automated providing real-time control and data reduction. That system will be briefly described in this report (see Fig. 1).

The calorimetric system contains two isolated electrical circuits, one for the measurement of the temperature of the calorimeter and the other to provide electrical power to calibrate the instrument and change the calorimeter temperature. Measurements in both circuits are made using the standard procedures for four lead voltage measurements across a resistance, that is, two leads provide the current path and two separate leads are used to monitor the potential drop across the resistance. A standard resistor (of known resistance at a fixed temperature and known temperature coefficient) is used in each circuit to derive the magnitude of the circuit current using Ohm's Law and the measured voltage at the standard resistor. Details of the calculations leading to heat-capacity date are given in Robie and Hemingway (1972).

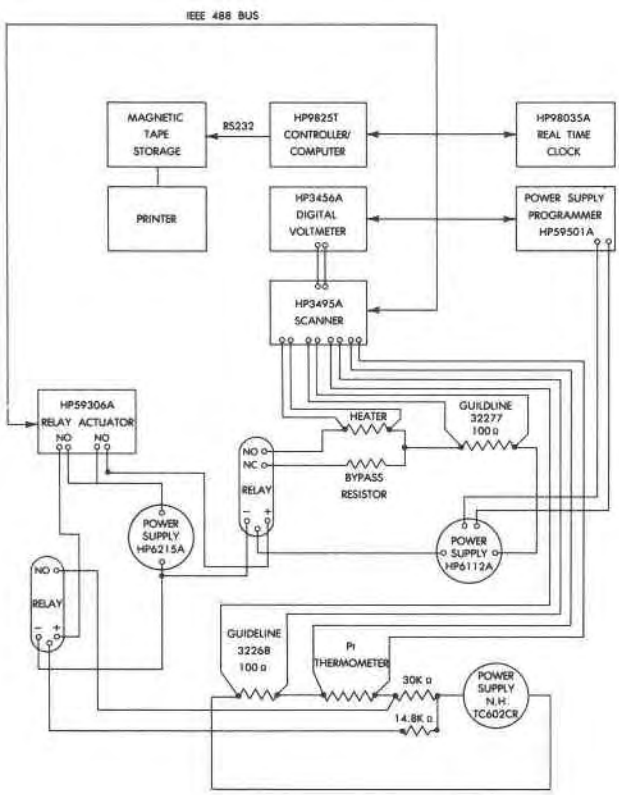

Fig. 1. Schematic diagram of the control circuit for the low-temperature calorimeter. The main components are described in the text. Additional details may be found in Robie and Hemingway (1972).

To control the collection of data from the low-temperature calorimeter, the system must be able to measure several voltages as a function of time, to adjust power applied during the electrical calibration (heat-capacity measurement) of the system, to actuate relays at specific points in the experiment, and vary parameters of the experiment as conditions change. A Hewlett-Packard (HP) 9825 desk-top computer programmed in HPL (copyright, Hewlett-Packard Desktop Computer Division, Fort Collins, CO) was chosen as the primary system control unit.

The control software is driven by 30 second interrupts provided by an HP98035A real-time clock. Elapsed time calculations, based upon these interrupts, may be made to ±0.005 seconds provided care is exercised in designing the program code. Determination of elapsed times in this manner eliminates the need for a separate interval timer (e.g., Robie et al., 1976).

Voltage measurements are made with a 6-1/2 digit HP3456A digital voltmeter using voltage signals supplied from an HP3495A scanner. The voltage leads from the four measurement resistors (see Fig. 1) are attached to low-thermal-emf, programmable relays in the scanner.

An HP59306A relay actuator provides programmable switch closures that are used in this system to increase the circuit current at temperatures below 37 K (to provide greater sensitivity in low temperature determinations) by energizing the coil of a mercury wetted relay, and to initiate and terminate the electrical calibration of the calorimeter. The mercury relays (Claire HGS-5000 series) have a throw time of 900 μs (microseconds) and a voltage drop at the switch contacts of 25 μV (microvolts) constant to ±5 μV.

The current supplied during the electrical calibration of the calorimeter can be preset using an HP59501A power supply programmer and an HP6112A power supply. There are 999 programmable settings between 0 mA (milliamps) and the maximum value preset for the power supply (60 mA in this system).

Data collected during the experiment are recorded on the internal magnetic tape cartridge in the HP9825 computer, on an external cartridge tape recorder (Tektronix 4923), and/or on a printer (HP2635A).

The preceding discussion provides a brief overview of the current data collecting system. The intent of the authors is to provide documentation of a significant change in the calorimetric system, without discussing the detail of the measurement theory or the calculations, both of which may be found in Robie and Hemingway (1972). The precision of the measurements is better than 0.3 percent for temperatures above 20 K, but decreases to ±10 percent at 4.5 K.

Heat capacities of osumilite

The heat capacities of a natural sample of osumilite ($K_{0.93}Na_{0.09}Ca_{0.02}Ba_{0.01}Mg_{1.88}Fe_{0.38}Ti_{0.01}Al_{4.62}Si_{10.12}O_{30}$)

were measured from 340 to 1000 K in a differential scanning calorimeter (DSC). The results were extrapolated to 298.15 K. Instability in the DSC reduced the quality of the data above 800 K.

The heat-capacity values were fit with an equation of the type suggested by Haas and Fisher (1976) with an average deviation of 0.5 percent. The experimental results are listed in Table 2 together with the polynomial representing the heat capacity of osumilite. The heat capacities have not been corrected for deviations from the theoretical endmember composition $KMg_2Al_3(Al_2Si_{10})O_{30}$ resulting from substitution of Si for Al, Fe for Mg, or Mg for Al. The heat-capacity values and the polynomial representing the data are, therefore, reported in units of joules per gram of natural sample.

The available amount of osumilite sample 2045C was not sufficient for our low-temperature adiabatic calorimeter. We also have a sample collected by E. S. Grew from a nearby locality, Mount Riiser-Larsen, Enderby Land, Antarctica, that will provide sufficient material for the low-temperature calorimeter. Thus, further work on sample 2045C is not warranted.

Table 2. Experimental specific heats of osumilite. (The equation fit the data with an average deviation of 0.5 percent.)

Temp.	Heat capacity	Temp.	Heat capacity	Temp.	Heat capacity
K	J/(g·K)	K	J/(g·K)	K	J/(g·K)
Series 1		Series 3		Series 5	
419.9	0.9105	419.9	0.9013	619.8	1.0500
429.9	0.9145	429.9	0.9170	629.8	1.0580
439.9	0.9163	439.9	0.9240	639.7	1.0630
449.9	0.9228	449.9	0.9251	649.7	1.0700
459.9	0.9423	459.9	0.9461	659.7	1.0760
469.9	0.9350	469.9	0.9383	669.7	1.0810
479.8	0.9503	479.9	0.9522	679.7	1.0850
489.8	0.9613	489.9	0.9575	689.7	1.0890
499.8	0.9744	499.8	0.9661	699.7	1.0930
509.8	0.9721	509.8	0.9701	709.7	1.0960
519.8	0.9766	519.8	0.9778	719.7	1.1020
529.8	0.9905	529.8	0.9962	729.7	1.1060
539.8	1.0100	539.8	1.0050	739.7	1.1080
549.8	1.0080	549.8	1.0120	749.7	1.1120
				759.7	1.1120
Series 2		Series 4		769.7	1.1150
				779.7	1.1170
339.9	0.8217	519.8	0.9959	789.7	1.1180
349.9	0.8337	529.8	1.0000	799.7	1.1200
359.9	0.8480	539.8	1.0070		
369.9	0.8577	549.8	1.0160	Series 6	
379.8	0.8685	559.8	1.0260		
389.8	0.8824	569.8	1.0250	889.0	1.1380
399.8	0.8927	579.8	1.0300	899.9	1.1440
409.8	0.9024	589.8	1.0330		
419.8	0.9128	599.8	1.0420	Series 7	
429.8	0.9200	609.8	1.0480		
439.8	0.9313	619.8	1.0510	997.8	1.1640
449.8	0.9400	629.8	1.0560		
		639.7	1.0570		
		649.7	1.0640		

$$C_p^\circ = 0.58332 + 1.2742 \times 10^{-3}T - 6.4871 \times 10^{-7}T^2 - 1.554T^{-0.5} - 3.961 \times 10^{3}T^{-2} \quad (298.15 \text{ to } 1000 \text{ K})$$

Heat capacities of two natural chlorites

The heat capacities of two natural chlorite samples have been measured from near 10 K to 380 K using the intermittent heating method under quasiadiabatic conditions in the cryostat described by Robie and Hemingway (1972) and using the automated data-collection system discussed in earlier sections of this paper. The heat capacities of the chlorites were measured between 340 and 500 K using a DSC and following the procedures of Krupka et al. (1979).

The low-temperature heat capacities were determined from measurements on samples of 18.2700 and 32.1432 g, respectively, for chlorites 21-C and 21-D (each corrected for bouyancy). Sample 21-C represented 50 percent of the measured heat capacity (sample plus calorimeter) at 10 K, 14 percent at 50 K, 20 percent at 100 K, 30 percent at 200 K, and 40 percent at 380 K. Sample 21-D represented 80 percent of the measured heat capacity at 15 K, 30 percent at 50 K, 40 percent at 180 K, and 50 percent at 350 K. The samples prepared for the DSC were 38.141 and 47.709 mg, respectively, for chlorites 21-C and 21-D. Adsorbed water was removed from sample 21-D before the DSC sample was weighed by heating the sample at 500 K in the DSC until the isothermal baseline became stable (i.e., until all water had been evaporated and a constant power input was established). The heat capacities of the two chlorite samples were measured with the petalite sample (discussed later) in successive scans, and therefore, each sample is referenced to the same thermal scans for the empty gold pan and the corundum standard (e.g., Krupka et al., 1979).

The measured heat capacities (corrected for curvature, e.g., Robie and Hemingway, 1972) are listed in Tables 3 and 4, grouped in the order in which the experiments were performed. Sample 21-C contained large, well-formed cleavage flakes that were of sufficient size to allow disks, equivalent in diameter to the DSC pans, to be cut with a cork bore for the DSC sample. The DSC heat-capacity values obtained from this sample were in excellent agreement with the results obtained with the low-temperature adiabatic calorimeter. Sample 21-D contained particles <104 μm and at the lowest temperatures (about 12 K and below) adsorption of the He exchange gas (e.g., Robie and Hemingway, 1972) became a significant problem. The heat-capacity values for sample 21-D obtained from the DSC show a significant (>0.5 percent) offset from the heat-capacity values obtained with the more accurate low-temperature calorimeter. Heat-capacity results obtained on powdered samples with a DSC, in general, are not as accurate as those obtained from samples in the form of single crystals or as several stacked disks of well-crystallized sheet-structure minerals.

Smoothed values of the thermodynamic properties of heat capacity, C_P°, entropy, $S_T^\circ - S_0^\circ$, enthalpy function, $(H_T^\circ - H_0^\circ)/T$, and Gibbs energy function, $(G_T^\circ - H_0^\circ)/T$, for

Table 3. Experimental heat capacities of 573.658 g of high-magnesium chlorite (sample 21-C).

Temp. K	Heat capacity J/(mol·K)	Temp. K	Heat capacity J/(mol·K)	Temp. K	Heat capacity J/(mol·K)
Series 1		Series 2		Series 3	
10.02	2.848	96.56	136.0	292.81	529.1
10.92	2.874	102.49	151.2	297.91	535.1
11.98	2.913	108.39	166.2	303.00	542.4
		114.23	181.4	308.53	549.7
Series 2		120.02	196.3	314.51	556.1
		125.76	210.2	320.47	562.6
4.99	3.417	131.47	225.0	326.42	569.9
5.39	2.679	137.15	238.2	332.35	575.8
6.10	2.503	142.78	252.5	338.26	582.1
6.77	2.651	148.40	264.7	344.16	588.2
7.46	2.783	153.95	277.4	349.03	595.0
8.24	2.833	159.50	291.0		
9.17	2.800	165.03	304.8	Series 4	
10.19	2.786	170.53	317.0		
11.28	2.920	176.02	329.0	354.48	601.1
12.47	3.015	181.48	340.5	359.37	605.6
13.78	3.198	186.92	351.0	364.26	610.4
15.24	3.501	192.36	361.6	369.22	614.7
16.84	3.897	197.76	372.7	374.16	620.4
18.61	4.444	203.16	382.5	379.09	624.2
20.59	5.201	208.54	392.7		
22.79	6.067	213.91	404.1	Series 5	
25.25	7.254	219.27	413.7		
28.01	8.900	224.64	422.1	340.0	583.7
31.09	11.39	230.02	432.1	350.0	593.7
34.56	14.69	235.40	441.4	360.0	603.9
38.45	19.69	240.77	451.7	370.0	613.4
42.80	25.15	246.14	460.1	380.0	622.0
47.69	31.57	251.49	467.6	390.0	632.2
53.15	40.76	256.82	475.5	400.0	639.5
59.18	50.89	262.14	484.0	410.0	648.3
65.54	63.75			420.0	657.2
71.91	77.81	Series 3		430.0	663.7
78.19	92.77			440.0	670.8
84.38	107.6	267.31	492.2	450.0	679.0
90.49	122.1	272.48	500.0	460.0	686.9
		277.52	506.8	470.0	690.8
		282.56	514.6	480.0	696.5
		287.69	522.3	490.0	704.0
				500.0	707.1

the two chlorite samples are listed in Tables 5 and 6 at integral temperatures between 0 and 370 K. These values are based upon estimates of the heat-capacity change between 0 and 5 K for sample 21-C and between 0 and about 12 K for sample 21-D, and are based upon the assumption that these estimated values combined with the measured data completely define the heat capacity associated with the spin energy contribution of the paramagnetic ions in the chlorite samples at the lowest temperatures (see discussion below). The measured heat-capacity results have not been corrected for the deviations from the idealized formulations derived by Kittrick (1982) and used in this paper. In the case of sample 21-D, the deviation from the end member composition (impurities, either from unrecognized impurity phases or as cation substitutions) represent about 10 percent of the sample and yield an average entropy per gram of impurity (calculated by oxide summation) that differs from the measured entropy per gram of sample by about 1 percent. Thus, for sample 21-D, a correction for the "impurities" would result in a change in the calculated entropy of less than 0.2 percent, a value less than the experimental uncertainty in the entropy. The "impurities" in sample 21-C represent about 0.6 percent. Corrections for these impurities will not produce a significant change in the calculated entropy.

When electrons move between a ground state and a higher energy state, the heat capacity records the change. Schottky (1922) was the first person to discuss this process and the anomalous patterns that would be reflected in the heat capacity. Such heat capacity anomalies are called Schottky anomalies and they may arise in paramagnetic crystalline phases from cooperative, non-cooperative, or a combination of the two processes of splitting spin states (see Gopal, 1966, for a detailed discussion of magnetic contributions to heat capacity and entropy). When the energy separations of the states are small, the anomalous heat capacities are observed at low temperatures often providing large contributions to the entropy below 10 K.

Table 4. Experimental heat capacities of 659.133 g of high-iron chlorite (sample 21-D).

Temp. K	Heat capacity J/(mol·K)	Temp. K	Heat capacity J/(mol·K)	Temp. K	Heat capacity J/(mol·K)
Series 2		Series 2			
				Series 4	
14.63	15.19	176.99	348.4		
16.94	16.88	182.44	359.8	353.23	600.0
19.17	18.71	187.88	370.0	358.17	605.4
21.32	20.68	193.31	380.1	363.01	609.5
23.66	22.98	198.72	390.1	367.86	615.0
26.21	25.75	204.11	399.6	372.78	619.8
29.03	29.14	209.48	408.5	377.68	626.0
32.19	33.43	214.84	417.5		
35.71	39.09	220.18	426.7	Series 5	
39.66	45.20	225.53	436.2		
44.09	52.92	230.88	444.8	340.00	579.4
49.05	61.11	236.23	453.4	350.00	589.0
54.60	70.95			360.00	598.3
60.66	82.29	Series 3		370.00	606.0
66.93	96.36			380.00	613.6
73.18	110.8	243.01	463.8	390.00	622.4
79.39	125.8	248.13	472.1	400.00	629.6
85.53	140.5	253.10	480.2	410.0	637.5
91.60	155.0	258.10	487.5	420.0	645.5
97.62	169.4	263.24	494.4	430.0	651.4
103.57	183.5	268.39	501.2	440.0	659.1
109.44	201.0	273.53	507.2	450.0	666.8
115.27	211.9	278.65	514.1	460.0	674.5
121.08	225.9	283.75	521.2	470.0	679.1
126.81	239.6	288.85	528.2	480.0	684.3
132.49	252.9	293.92	535.3	490.0	691.7
138.15	265.9	298.99	540.5	500.0	695.7
143.77	278.5	304.04	547.1		
149.37	290.7	309.07	553.3	Series 1	
154.95	302.6	314.10	558.4		
160.50	314.5	319.11	563.5	11.05	4.327
166.02	326.3	324.10	569.6	11.29	8.018
171.52	336.9	329.07	574.7	12.63	12.71
		334.04	581.8		
		339.00	586.9		
		343.97	592.1		
		348.96	596.3		

Table 5. Thermodynamic properties of 573.658 g of high-magnesium chlorite (sample 21-C). (For this tabulation, the zero-point entropy is 0.)

Temp.	Heat capacity	Entropy	Enthalpy function	Gibbs energy function
T	C_P°	$S_T^\circ - S_0^\circ$	$(H_T^\circ - H_0^\circ)/T$	$-(G_T^\circ - H_0^\circ)/T$
Kelvin		J/(mol·K)		
5	2.725	0.756	0.638	0.118
10	2.826	2.660	1.695	0.965
15	3.441	3.888	2.147	1.741
20	4.945	5.065	2.642	2.423
25	7.127	6.389	3.308	3.081
30	10.46	7.960	4.201	3.759
35	15.31	9.917	5.423	4.494
40	21.34	12.35	7.027	5.319
45	28.01	15.24	8.983	6.256
50	35.42	18.57	11.25	7.318
60	52.82	26.51	16.68	9.831
70	73.52	36.17	23.29	12.88
80	96.51	47.47	30.99	16.48
90	120.6	60.22	39.60	20.62
100	145.2	74.20	48.92	25.27
110	170.4	89.22	58.82	30.40
120	195.7	105.1	69.17	35.95
130	220.7	121.8	79.87	41.91
140	245.2	139.0	90.81	48.23
150	269.1	156.8	101.9	54.87
160	292.4	174.9	113.1	61.81
170	315.0	193.3	124.3	69.00
180	336.6	211.9	135.5	76.42
190	357.3	230.7	146.6	84.04
200	377.1	249.5	157.7	91.85
210	396.2	268.4	168.6	99.80
220	414.6	287.2	179.3	107.9
230	432.3	306.1	190.0	116.1
240	449.3	324.8	200.4	124.4
250	465.6	343.5	210.7	132.8
260	481.3	362.1	220.8	141.3
270	496.4	380.5	230.7	149.8
280	510.9	398.8	240.5	158.3
290	524.7	417.0	250.0	167.0
300	537.9	435.0	259.4	175.6
325	568.2	479.3	282.0	197.3
350	595.2	522.4	303.5	218.9
375	619.4	564.3	323.7	240.6
400	640.7	605.0	342.9	262.1
425	660.3	644.4	361.0	283.4
450	678.1	682.7	378.1	304.5
475	694.3	719.8	394.3	325.4
500	709.6	755.8	409.7	346.0
273.15	501.0	386.3	233.8	152.5
298.15	535.6	431.7	257.7	174.0

Both chlorite samples exhibit a Schottky anomaly. For sample 21-D, the anomaly is large and poorly defined on the low-temperature side as a result of the adsorption of the He exchange gas at temperatures less than 12 K. The heat-capacity curve derived from our measurements of sample 21-C shows a well defined Schottky anomaly centered at about 8 K and a lower temperature anomaly. At the lowest temperatures of our measurements of sample 21-C, the heat capacity was increasing. Therefore, the lower temperature peak was not completely defined by our measurements.

Separation of the Schottky heat capacity is difficult, but it is necessary to at least estimate the contribution in order to determine the uncertainty of the measured entropy. Hemingway and Robie (1984) have reviewed several methods that have been devised to separate the lattice heat capacity from the measured heat capacity; however, none of these methods is directly applicable to analyses of the chlorites. Modifying one of the commonly used methods (corresponding states procedure e.g., Lyon and Giauque, 1949) will allow us to make a first approximation of the lattice heat capacity of the chlorite samples.

The lattice heat capacity of a phase exhibiting a Schottky anomaly is often approximated by the scaled heat capacity of a diamagnetic reference phase with a

Table 6. Thermodynamic properties of 659.133 g of high-iron chlorite (sample 21-D). (For this tabulation, the zero-point entropy is 0.)

Temp.	Heat capacity	Entropy	Enthalpy function	Gibbs energy function
T	C_P°	$S_T^\circ - S_0^\circ$	$(H_T^\circ - H_0^\circ)/T$	$-(G_T^\circ - H_0^\circ)/T$
Kelvin		J/(mol·K)		
5	0.064	0.020	0.014	0.006
10	1.422	0.261	0.209	0.052
15	15.48	4.394	3.708	0.686
20	19.62	9.351	7.116	2.235
25	24.72	14.26	10.11	4.149
30	30.74	19.29	13.04	6.251
35	37.69	24.54	16.05	8.485
40	45.42	30.07	19.23	10.83
45	53.77	35.89	22.60	13.29
50	62.66	42.01	26.16	15.86
60	82.08	55.12	33.83	21.29
70	103.5	69.36	42.23	27.13
80	126.6	84.68	51.32	33.35
90	150.5	101.0	61.01	39.95
100	174.8	118.1	71.17	46.90
110	199.1	135.9	81.70	54.18
120	223.1	154.2	92.48	61.75
130	246.6	173.0	103.4	69.58
140	269.5	192.1	114.5	77.65
150	291.7	211.5	125.6	85.93
160	313.3	231.0	136.6	94.38
170	334.1	250.6	147.6	103.0
180	354.1	270.3	158.6	111.7
190	373.4	290.0	169.4	120.6
200	392.0	309.6	180.0	129.6
210	409.9	329.2	190.5	138.6
220	427.0	348.6	200.9	147.7
230	443.6	368.0	211.1	156.9
240	459.5	387.2	221.1	166.1
250	474.8	406.3	231.0	175.3
260	489.5	425.2	240.6	184.5
270	503.5	443.9	250.1	193.8
280	517.1	462.5	259.4	203.1
290	530.0	480.8	268.5	212.3
300	542.4	499.0	277.4	221.6
325	571.0	543.6	298.9	244.6
350	595.7	586.8	319.3	267.5
375	616.5	628.7	338.4	290.2
400	634.3	669.0	356.4	312.7
425	650.8	708.0	373.2	334.8
450	666.7	745.6	389.1	356.6
475	682.2	782.1	404.1	378.0
500	697.6	817.5	418.4	399.1
273.15	507.9	449.8	253.1	196.7
298.15	540.2	495.7	275.8	219.9

similar crystal structure that does not have an anomaly. We do not have the heat capacity of a chlorite that is free of paramagnetic ions to use for this model. Therefore, we will modify the method and use the sum of the heat capacities of one talc and three brucite to represent the reference phase. Scaling of the reference or model heat-capacity data is accomplished by plotting (see Fig. 2) the ratio of the heat capacity of the chlorite divided by the heat capacity of the reference phase at the same temperature, for temperatures to several hundreds of degrees above the region of the Schottky anomaly (e.g., Lyon and Giauque, 1949). Where the data exhibit a linear trend with temperature, the ratio is assumed to represent conditions where all energy levels are occupied and the Schottky effect represents a constant contribution to the entropy. From the data presented in Figure 2, we can estimate lattice heat-capacity values for sample 21-C from the equation derived from the data in the temperature range from 180 to 300 K, and for sample 21-D from the equation for the data in the temperature range from 180 to 250 K. The approximation for sample 21-D is obviously not good and the region chosen for the scaling equation was selected simply to be consistent with that chosen for sample 21-C. The heat capacity of talc was taken from the data of Robie and Stout (1963) and the heat capacity of brucite was from the report by Giauque and Archibald (1937) and an estimate of the heat capacity of $Mg(OH)_2$ between 0 and 22 K made for this model.

The entropies associated with the Schottky peaks were calculated by integrating the heat capacities representing the difference between the measured chlorite heat capacities and the scaled model heat capacities representing the chlorite lattice. The measured heat capacities were extrapolated to 0 K by assuming that the heat capacity of sample 21-D dropped rapidly from its peak value at about 14 K (in a plot of Cp/T vs. T^2) and by assuming that sample 21-C exhibited cooperative ordering of spins at about 4.7 K and was approximated by a small λ-type peak in the heat capacity. This latter effect could also result from the splitting of a lower doublet of the ground state quintet of Fe^{2+} as found in the work of Hill and Smith (1953); however, the difference in interpretation is not relevant to the estimate of the heat capacity used in this study.

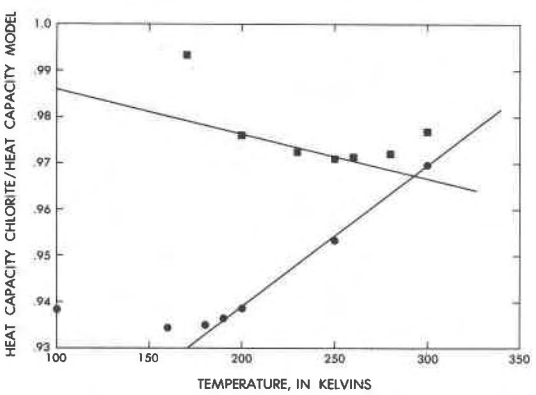

Fig. 2. Schematic diagram of the model used to estimate the lattice contribution to the heat capacities of chlorites 21-C (circles) and 21-D (squares). A description of the procedure is given in the text.

For comparison, the theoretical magnetic entropy contribution was calculated for each chlorite by assuming that the crystalline field surrounding each paramagnetic ion in the chlorite was of sufficiently low symmetry to remove the orbital degeneracy of the ground states of the ions and that the orbital angular momentum of the ground state of each of the free paramagnetic ions was quenched, i.e., the spin quantum numbers used were $s = 2$ for Fe^{2+} and $s = 5/2$ for Fe^{3+} and Mn^{2+}, and the molar magnetic entropy per paramagnetic ion was equal to $R\ln(2s + 1)$ (e.g., Gopal). Magnetic entropies calculated for temperatures between 0 and 200 K for each chlorite were divided by the total theoretical magnetic contribution expected for that chlorite and were plotted in Figure 3. If one considers the uncertainties associated with the differences between the measured chlorite heat capacities and the estimates of the heat capacities for each chlorite lattice, the results may be considered to agree with the theoretical values within the experimental error. However, this analysis is not sufficiently accurate to rule out additional magnetic entropy contributions for temperatures below the lowest measurements of this study.

The DSC heat-capacity values were combined with the heat-capacity data obtained at temperatures higher than 200 K by low-temperature adiabatic calorimetry and fit to an equation of the form suggested by Haas and Fisher (1976). The data for chlorite 21-C were fit by the polynomial

$$C_P^\circ = 1948.911 - 0.580880T + 2.0897 \times 10^{-4}T^2 - 2.298327 \times 10^4 T^{-0.5} + 6.42272 \times 10^6 T^{-2}$$

with an average deviation of 0.14 percent. The heat capacities of chlorite 21-D were fit by the polynomial

$$C_P^\circ = 3639.373 - 2.588354T + 1.26827 \times 10^{-3}T^2 - 4.564707 \times 10^4 T^{-0.5} + 1.80322 \times 10^7 T^{-2}$$

with an average deviation of 0.36 percent. Both equations are valid from 200 to 500 K.

The entropies at 298.15 K of 431.7±5.0 and 495.7±10 J/(mol · K), respectively, for chlorites 21-C and 21-D do not contain configurational entropy contributions. An extensive discussion of the problems of order–disorder in chlorites may be found in Bailey (1975). Because we do not have information on the site-occupany of the chlorites we have not estimated the zero-point entropy. Also lacking estimates of the mixing terms we have not at-

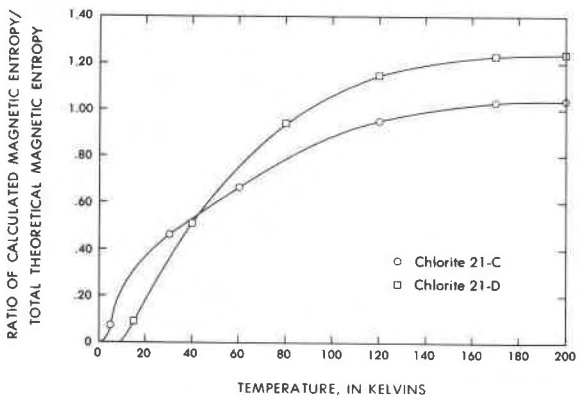

Fig. 3. Representation of the estimated entropy contribution of the low-temperature Schottky heat-capacity anomalies. The results are presented as a ratio of the entropy calculated at each temperature from the difference between the measured heat capacities and the heat capacity estimated from the model used for the lattice contribution (see description in text) divided by the total theoretical magnetic entropy. If the calculations properly reflect the magnetic heat capacities of the chlorites, the ratio should approach unity at the higher temperature where the split levels should be fully occupied.

tempted to correct these values to end-member compositions.

Thermodynamic properties of petalite

The heat capacities of petalite, $LiAlSi_4O_{10}$, have been measured from 4.5 to 380 K using the intermittent heating method under quasi-adiabatic conditions in the cryostat described by Robie and Hemingway (1972) and using the automated data-collection system discussed in earlier sections of this paper. The heat capacities of petalite were measured between 340 and 500 K using a DSC and following the procedures of Krupka et al. (1979).

The low-temperature heat capacities were determined from measurements on a sample of 36.0596 g (corrected for buoyancy). The petalite sample represented 40 percent of the total measured heat capacity (sample plus calorimeter) at 4.5 K and 50 percent at 380 K. The petalite sample prepared for the DSC measurements was 36.199 mg. The DSC sample (three large grains each having one flat side) was placed in a covered gold pan. The heating rate was 10 K/min and the sensitivity was 20.9 mJ/sec.

The measured heat capacities (corrected for curvature, e.g., Robie and Hemingway, 1972) are listed in Table 7, grouped in the order in which the experiments were performed. The DSC results represent the average values from two scans from 340 to 500 K.

The molar thermodynamic properties for petalite are listed in Tables 8 and 9 using 306.2585 g as the gram formula weight. The results listed in Table 8 are calculated from the experimental data listed in Table 7 and an extrapolation of the measurements to 0 K. The values listed in Table 9 represent a simultaneous fit to the low-temperature heat-capacity data for temperatures higher than 200 K, the DSC data, and the heat-content data reported by Bennington et al. (1980). For temperatures higher than 1200 K, the heat capacity of petalite was estimated as the sum of the heat capacities of the oxide components, 1/2 corundum, 1/2 Li_2O, and 4 coesite (Robie et al., 1979). The sum of these components agreed with the smoothed heat capacities reported by Bennington et al. to better than 0.15 percent in the temperature range 900 to 1200 K.

The polynomial $C_P^\circ = 876.26 - 0.20793\ T + 5.3009 \times 10^{-5}T^2 - 1.0691 \times 10^4 T^{-0.5} + 4.033 \times 10^6 T^{-2}$ fits the data to ±0.17 percent and is valid for the temperature interval 200 to 1800 K.

Roy et al. (1950) have shown that natural petalite will decompose to spodumene above 950 K and about 1 kbar. Bennington et al. (1980) found substantial β-spodumene in their sample when the material was heated to 1200 K. London (1981) has studied the stability field for petalite with experiments at 2 and 4 kbar and temparatures to 1000 K. The preliminary results of recent work appear to

Table 7. Experimental heat capacities for 306.2585 g of petalite.

Temp. K	Heat capacity J/(mol·K)	Temp. K	Heat capacity J/(mol·K)	Temp. K	Heat capacity J/(mol·K)
Series 1		Series 1		Series 2	
4.51	0.1912	110.47	97.50	297.75	245.5
5.27	0.1260	116.42	103.7	303.03	248.3
5.58	0.0821	122.32	110.6	308.31	250.8
6.01	0.1265	128.18	116.1	313.56	253.2
6.42	0.1548	134.02	122.0	318.80	255.5
6.97	0.2117	139.84	127.9	324.01	258.3
7.62	0.2908	145.64	133.4	329.23	260.9
8.35	0.4065	151.41	139.0	334.43	263.8
9.19	0.5832	157.16	144.3	339.62	265.8
10.14	0.8302	162.89	149.7	344.81	268.7
11.21	1.174	168.61	154.6	350.00	270.6
12.41	1.653			355.18	273.2
13.75	2.303	Series 2		360.34	275.4
15.25	3.152			365.49	277.7
16.95	4.239	174.23	159.6	370.62	280.0
18.83	5.602	179.71	164.4	375.74	282.6
20.94	7.249	184.90	168.7	380.84	284.1
23.30	9.161	190.14	172.8		
25.92	11.38	195.62	177.4	Series 3	
28.85	13.94	201.07	181.8		
32.11	16.96	206.52	185.8	340.0	266.5
35.74	20.59	211.96	189.8	350.0	270.4
39.80	24.31	217.37	193.8	360.0	274.5
44.34	28.68	222.78	197.8	370.0	278.3
49.40	33.25	228.18	201.6	380.0	282.4
55.03	38.45	233.58	205.7	390.0	287.2
61.16	44.61	238.98	208.7	400.0	290.4
67.46	51.18	244.37	212.0	410.0	294.4
73.76	58.05	249.75	215.9	420.0	298.0
80.02	64.91	255.12	219.6	430.0	301.4
86.21	71.54	260.47	223.0	440.0	305.1
92.35	78.13	265.83	226.1	450.0	309.4
98.43	84.99	271.19	229.1	460.0	313.3
104.48	91.23	276.53	232.2	470.0	317.3
		281.86	235.7	480.0	318.8
		287.17	238.8	490.0	322.3
		292.47	242.2	500.0	325.0

confirm Stewart's (1963) observation that petalite is unstable above approximately 975 K at any pressure (D. London, unpub. data, 1982). Under quartz-saturated conditions, the conversion of petalite to β-spodumene consumes quartz and produces a tetragonal β-spodumene phase of an approximate composition of $Li_2Al_2Si_9O_{22}$ (D. London, unpub. data, 1982). The composition of this phase appears to be fixed under quartz-saturated conditions (i.e., at constant activity of SiO_2, see also, Skinner and Evans, 1960).

Conclusion

The thermodynamic properties of petalite reported in this study confirm the earlier work of Bennington et al. (1980).

Table 8. Thermodynamic properties of 306.2585 g of petalite at lower temperatures.

Temp.	Heat capacity	Entropy	Enthalpy function	Gibbs energy function
T	C_P°	$S_T^\circ - S_0^\circ$	$(H_T^\circ - H_0^\circ)/T$	$-(G_T^\circ - H_0^\circ)/T$
Kelvin		J/(mol·K)		
5	0.072	0.022	0.017	0.005
10	0.791	0.221	0.171	0.050
15	2.999	0.905	0.700	0.205
20	6.491	2.223	1.691	0.532
25	10.58	4.105	3.054	1.051
30	15.02	6.421	4.674	1.748
35	19.77	9.091	6.488	2.602
40	24.53	12.04	8.447	3.595
45	29.21	15.20	10.49	4.708
50	33.83	18.52	12.60	5.922
60	43.47	25.53	16.93	8.599
70	53.93	33.00	21.46	11.55
80	64.80	40.91	26.19	14.72
90	75.67	49.17	31.09	18.08
100	86.48	57.71	36.09	21.62
110	97.13	66.45	41.15	25.30
120	107.7	75.36	46.26	29.09
130	118.0	84.39	51.39	33.00
140	128.0	93.50	56.50	37.00
150	137.6	102.7	61.59	41.07
160	146.9	111.8	66.64	45.20
170	155.9	121.0	71.63	49.39
180	164.5	130.2	76.55	53.63
190	172.8	139.3	81.40	57.90
200	180.8	148.4	86.17	62.19
210	188.4	157.4	90.86	66.51
220	195.8	166.3	95.47	70.85
230	202.8	175.2	99.98	75.19
240	209.6	183.9	104.4	79.54
250	216.1	192.6	108.7	83.89
260	222.4	201.2	113.0	88.24
270	228.6	209.7	117.2	92.58
280	234.7	218.2	121.3	96.91
290	240.6	226.5	125.3	101.2
300	246.2	234.8	129.2	105.6
310	251.5	242.9	133.1	109.9
320	256.5	251.0	136.8	114.1
330	261.4	259.0	140.5	118.4
340	266.1	266.8	144.2	122.7
350	270.8	274.6	147.7	126.9
360	275.3	282.3	151.2	131.1
370	279.7	289.9	154.6	135.3
380	284.1	297.4	158.0	139.5
273.15	230.5	212.4	118.5	93.95
298.15	245.2	233.2	128.5	104.8

Table 9. Thermodynamic properties of 306.2585 g of petalite at higher temperatures. [The results are calculated from DSC measurements to 500 K, heat-content data to 1200 K (Bennington et al., 1980), and estimated values from 1200 K to 1800 K calculated as the sum 1/2 corundum + 1/2 Li_2O + 4 coesite (Robie et al., 1979).]

Temp.	Heat Capacity	Entropy	Enthalpy Function	Gibbs energy Function
T	C_P°	S_T°	$(H_T^\circ - H_{298}^\circ)/T$	$-(G_T^\circ - H_{298}^\circ)/T$
Kelvin		J/(mol·K)		
298.15	245.2	233.2	0.0	233.2
300	246.2	234.7	1.5	233.2
350	271.5	274.6	38.3	236.3
400	292.2	312.3	68.8	243.5
450	309.4	347.7	94.6	253.1
500	323.6	381.1	116.8	264.2
550	335.4	412.5	136.2	276.3
600	345.3	442.1	153.2	288.9
650	353.7	470.1	168.3	301.8
700	360.8	496.6	181.8	314.8
750	366.9	521.7	194.0	327.7
800	372.2	545.5	204.9	340.6
850	376.7	568.2	214.9	353.3
900	380.7	589.9	224.0	365.9
950	384.2	610.6	232.4	378.2
1000	387.3	630.3	240.0	390.3
1050	390.1	649.3	247.1	402.2
1100	392.7	667.5	253.7	413.9
1150	395.0	685.0	259.8	425.3
1200	397.3	701.9	265.4	436.4
1250	399.4	718.1	270.8	447.4
1300	401.4	733.8	275.7	458.1
1350	403.4	749.0	280.4	468.6
1400	405.4	763.7	284.9	478.9
1450	407.4	778.0	289.1	488.9
1500	409.4	791.8	293.0	498.8
1550	411.4	805.3	296.8	508.5
1600	413.6	818.4	300.4	518.0
1650	415.8	831.2	303.9	527.3
1700	418.1	843.6	307.2	536.4
1750	420.5	855.8	310.4	545.3
1800	423.0	867.6	313.5	554.1

The thermodynamic properties reported for osumilite and chlorite represent initial results from an ongoing study of these minerals. The entropies reported for chlorite samples 21-C and 21-D most probably represent minimum entropies for those chemical compositions.

References

Bailey, S. W. (1975) Chlorites in Soil Components. Volume 2. Inorganic Components. Springer-Verlag, New York.

Bennington, K. O., Stuve, J. M., and Ferrante, M. J. (1980) Thermodynamic properties of petalite ($Li_2Al_2Si_8O_{20}$). U.S. Bureau of Mines Report of Investigations 8451.

Giauque, W. F. and Archibald, R. C. (1937) The entropy of water from the third law of thermodynamics. The dissociation pressure and calorimetric heat of the reaction $Mg(OH)_2 = MgO + H_2O$. The heat capacities of $Mg(OH)_2$ and MgO from 20 to 300° K. Journal of the American Chemical Society, 59, 561–569.

Gopal, E. S. R. (1966) Specific heats at low temperature. Plenum Press, New York.

Grew, E. S. (1982) Osumilite in the sapphirine–quartz terrane of Enderby Land, Antarctica: implications for osumilite petrogenesis in the granulite facies. American Mineralogist, 67, 762–787.

Haas, J. L., Jr. and Fisher, J. R. (1976) Simultaneous evaluation and correlation of thermodynamic data. American Journal of Science, 276, 525–545.

Hemingway, B. S. and Robie, R. A. (1984) Heat capacity and thermodynamic functions for gehlenite and staurolite with comments on the Schottky anomaly in the heat capacity of staurolite. American Mineralogist, 69, 307–318.

Hill, R. W. and Smith, P. L. (1953) The anomalous specific heat of ferrous ammonium sulphate. Physical Society of London, Proceedings A, 66, 228–232.

Jackson, M. L. (1969) Soil chemical analysis. Advanced course. 2nd edition, published by author, University of Wisconsin, Madison, WI.

Kittrick, J. A. (1982) Solubility of two high-Mg and two high-Fe chlorites using multiple equilibria. Clays and Clay Minerals, 30, 167–179.

Krupka, K. M., Robie, R. A., and Hemingway, B. S. (1979) High-temperature heat capacities of corundum, periclase, anorthite, $CaAl_2Si_2O_8$ glass, muscovite, pyrophyllite, $KAlSi_3O_8$ glass, grossular, and $NaAlSi_3O_8$ glass. American Mineralogist, 64, 86–101.

London, D. (1981) Preliminary experimental results in the system $LiAlSiO_4$–SiO_2–H_2O. Carnegie Institution of Washington Yearbook, 80, 341–345.

London, D. and Burt, D. M. (1982) Lithium aluminosilicate occurrences in pegmatites and the lithium aluminosilicate phase diagram. American Mineralogist, 67, 483–493.

Lyon, D. N. and Giauque, W. F. (1949) Magnetism and the third law of thermodynamics. Magnetic properties of ferrous sulfate heptahydrate from 1 to 20°K. Heat capacity from 1 to 310°K. Journal of the American Chemical Society, 71, 1647–1657.

Robie, R. A. and Hemingway, B. S. (1972) Calorimeters for heat of solution and low-temperature heat capacity measurements. U.S. Geological Survey Professional Paper 755.

Robie, R. A., Hemingway, B. S., and Fisher, J.R. (1979) Thermodynamic properties of minerals and related substances at 298.15 K and 1 bar (10^5 Pascals) pressure and at higher temperatures. U.S. Geological Survey Bulletin 1452 (originally printed 1978, revised).

Robie, R. A., Hemingway, B. S., and Wilson, W. H. (1976) The heat capacities of Calorimetry Conference copper and of muscovite $KAl_2(AlSi_3)O_{10}(OH)_2$, pyrophyllite $Al_2Si_4O_{10}(OH)_2$, and illite $K_3(Al_7Mg)(Si_{14}Al_2)O_{40}(OH)_8$ between 15 and 375 K and their standard entropies at 298.15 K. U.S. Geological Survey Journal of Research, 4, 631–644.

Robie, R. A., Hemingway, B. S., and Wilson, W. H. (1978) Low-temperature heat capacities and entropies of feldspar glasses and of anorthite. American Mineralogist, 63, 109–123.

Robie, R. A. and Stout, J. W. (1963) Heat capacity from 12 to 305°K and entropy of talc and tremolite. Journal of Physical Chemistry, 67, 2252–2256.

Roth, C. B., Jackson, M. L., Lotse, E. G., and Syers, J. K. (1968) Ferrous-ferric ratio and CEC changes on deferation of weathered micaceous vermiculite. Israel Journal of Chemistry, 6, 261–273.

Roy, R., Roy, D. M., and Osborn, E. F. (1950) Compositional and stability relationships among the lithium aluminosilicates: eucryptite, spodumene, and petalite. Journal of the American Ceramic Society, 33, 152–159.

Schottky, W. (1922) Über die Drehung der Atomachsen in festen Körpen. (M.t magnetischen, thermischen, und chemischen Beziehungen.) Physikalische zeitschrift, 23, 448–455.

Skinner, B. J. and Evans, H. T. (1960) β-spodumene solid solutions on the join Li_2O–Al_2O_3–SiO_2. American Journal of Science, 258A, 312–324.

Stewart, D. B. (1963) Petrogenesis and mineral assemblages of the lithiumrich pegmatites. (abstr.) Geological Society of America Special Paper 76, 159.

Manuscript received, March 3, 1983;
accepted for publication, January 2, 1984.